Hindawi
Wireless Communications and Mobile Computing
Volume 2018, Article ID 7846936, 9 pages
https://doi.org/10.1155/2018/7846936

Research Article

Measurement Method of Temporal Attenuation by Human Body in Off-the-Shelf 60 GHz WLAN with HMM-Based Transmission State Estimation

Yusuke Koda, Koji Yamamoto, Takayuki Nishio, and Masahiro Morikura

Graduate School of Informatics, Kyoto University, Yoshida-honmachi, Sakyo-ku, Kyoto 606-8501, Japan

Correspondence should be addressed to Yusuke Koda; koda@imc.cce.i.kyoto-u.ac.jp

Received 28 September 2017; Revised 15 February 2018; Accepted 20 March 2018; Published 23 April 2018

Academic Editor: Ahmed M. Al-Samman

This paper discusses a measurement method of time-variant attenuation of IEEE 802.11ad wireless LAN signals in the 60 GHz band induced by human blockage. The IEEE 802.11ad access point (AP) transmits frames intermittently, not continuously. Thus, to obtain the time-varying signal attenuation, it is required to estimate the duration in which the AP transmitted signals. To estimate whether the AP transmitted signals or not at each sampling point, this paper applies a simple two-state hidden Markov model. In addition, the validity of the model is tested based on Bayesian information criterion in order to prevent model overfitting and consequent invalid results. The measurement method is validated in that the distribution of the time duration in which the signal attenuates by 5 dB is consistent with the existing statistical model and the range of the measured time duration in which the signal attenuation decreases from 5 dB to 0 dB is similar to that in the previous report.

1. Introduction

A millimeter wave (mmWave) wireless LAN (WLAN) that leverages a channel bandwidth of over 2 GHz offers multi-gigabit data transfers, which attracts a lot of attention [1–4]. However, the mmWave WLAN experiences more signal attenuation induced by human blockage than WLANs that operate at the microwave band [5]. The attenuation is attributable to the use of higher directional antennas that are to compensate for a larger pass loss and to propagation characteristics of mmWave [6].

Many studies have suggested that communication devices perform a reactive action to respond to the human blockage [2, 7–9]. For example, the beam steering is an effective technique to overcome human blockage [2]. When the signal degradation is detected, the beam is switched at the direction in which a communication link utilizing reflected path without human blockage can be established. The authors in [8] proposed a multiband WLAN where a mmWave WLAN cooperates with a WLAN that operates at the 5 GHz band. They proposed changing the operating frequency to 5 GHz and thereby recovering the link quality when the human blockage is detected in the mmWave WLAN.

These reactive actions should be performed before the signal attenuates by an unacceptable threshold level. For example, when the signal attenuates by 5 dB, the physical layer (PHY) data rate is decreased by up to 2 Gbit/s [10], which can be a crucial problem for services that require high data rate. To do this, the period of monitoring received signal strength is to be smaller than the time span in which the signal attenuates by the threshold. In order to determine an appropriate period of the monitoring, characteristics of time-variant signal attenuation in the mmWave band induced by human bodies should be fully investigated.

The measurement of the time-variant signal attenuation in the millimeter wave band has been conducted in many studies [6, 11–17]. The authors in [13] measured the attenuation in the 60 GHz band and then compared the results with a knife edge diffraction model where the human body is modeled by two cylinders. The authors in [11] measured statistical characteristics of the time duration in which the signal attenuates by 5 dB, the time duration in which the signal attenuation level recovers from 5 dB to 0 dB, and time duration in which the human blockage event continues. From these parameters, they built a piecewise linear model for the time series of the signal attenuation in 60 GHz.

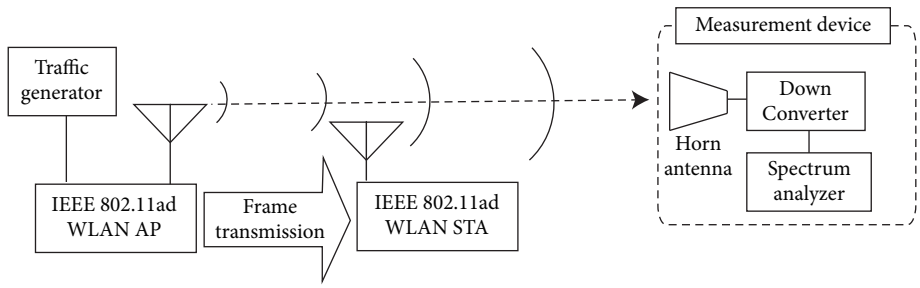

Figure 1: Block diagram of measurement system.

These measurements generally have employed horn antennas in a transmitter, while transmitters in mmWave WLANs employ consumer-grade array antennas to perform beamforming [4]. The authors in [5] revealed a significant difference between these two types of antennas in terms of directivity and side lobes. The difference between two types of antennas might give rise to the gap between the measurement results because antenna pattern of the transmitters gives an impact on the time series of signal attenuation [16]. For practical operation of mmWave WLANs, the gap should be investigated using a commercially available IEEE 802.11ad WLAN access point (AP) as a transmitter.

Being different from many measurements above where transmitters transmit continuous waves to receivers, the measurement of signals transmitted by an IEEE 802.11ad WLAN AP requires the estimation of whether the AP transmits signals or not at each sampling point in a sweep. This is due to the transmission mechanism of the AP. The AP transmits signals intermittently to a station (STA) according to medium access control (MAC) protocols [10]. The durations in which the AP transmits a signal might be smaller than a sweep length; hence, in each sweep length, there exist both durations in which the AP transmitted signals and durations in which the AP did not. Thus, in order to temporally track the signal attenuation due to human blockage, it is required to classify the samples into samples in the former durations and samples in the later durations.

In order to classify time-dependent variables, hidden Markov models (HMMs) are widely used in cognitive radio networks [18, 19]. The HMMs allow us to consider dependence between classes of subsequent values; thus, many studies have applied the HMM to the classification of time-dependent variables, in which there often exists dependence between subsequent values. In [18], the authors presented the method to estimate whether the interference signals exist or not in each time slot from overall samples in each slot. These studies have assumed that whether interference signals exist in each sample or not is identical in each time slot. This assumption is reasonable for time division multiple access, where the transmission time is slotted, and whether interference signals exist or not is identical in each time slot. However, the same way is not applicable to estimate whether WLAN signals exist or not in obtained samples because the transmission in WLANs is not slotted and in a sweep length there might exist both durations when the signals are present and those when the signals are absent.

In this paper, we conduct a measurement of time-varying signal attenuation induced by human blockage, involving a commercially available IEEE 802.11ad WLAN AP and STA. We present the estimation of whether signal is present or not at each sampling point using a simple two-state hidden Markov model. Being different from above-mentioned studies, we estimate classes, that is, signal presence or absence of *each* sample, not those of *overall* samples in a sweep length.

The contributions of this paper are threefold:

(i) In order to estimate whether the AP transmitted frames or not at each sampling point, we apply a simple two-state HMM.

(ii) Applying a two-state HMM to data obtained when the AP does not transmit any signals causes model overfitting and consequent invalid power calculation. Thus, we perform Bayesian information criterion-(BIC-) based model selection, where we select which two-state HMM or one-state model is more applicable to obtained data. We thereby detect this kind of the data and prevent model overfitting.

(iii) Our measurements are validated in that the statistical characteristics of the duration in which the signal attenuates by 5 dB are consistent with the statistical model built in a previous report, and the range of the duration in which the signal attenuation decreases from 5 dB to 0 dB is similar to that in the report.

The rest of this paper is organized as follows. Section 2 presents the architecture of our measurement system in detail. Section 3 presents the method to obtain the time-varying attenuation, involving an estimation of whether the AP transmitted a frame or not using HMM. Section 4 shows the measurement results. Section 5 concludes the paper.

2. Measurement Setup

Figure 1 shows the measurement system. The horn antenna receives radio frequency (RF) signals at 60.48 GHz, where the antenna is affixed to a waveguide flange input on the down converter. Then, the down converter converts the RF signal to a baseband signal. The microwave spectrum analyzer filters I-channel components of the baseband signal at the center frequency of 100 MHz with a bandwidth of 10 MHz. These signals are then sampled by an A/D converter in a spectrum analyzer. Figures 2 and 3 show pictures of the measurement

Table 1: Measurement equipment.

IEEE 802.11ad WLAN AP	Dell Wireless Dock D5000
IEEE 802.11ad WLAN STA	Dell Latitude E5540
Client laptop	Dell Latitude E5540
Wired network	1000BASE-T Gigabit Ethernet
Microwave spectrum analyzer	Tektronix RSA306
Down converter	Sivers IMA FC2221V
Antenna	Sivers IMA Horn antenna, 24 dBi

Table 2: Measurement parameters.

Channel	60.48 GHz
Sampling frequency $1/T$	14 MHz
Receiver antenna gain	24 dBi
Acquisition bandwidth	10 MHz
Number of samples per sampling K	2800

system and the measurement device, respectively. Details regarding the measurement equipment and the measurement parameters are shown in Tables 1 and 2, respectively.

Note that the choice of the bandwidth, which is smaller than the IEEE 802.11ad WLAN channels, is attributed to the time resolution in which we obtain the signal attenuation. In order to show the consistency in the time duration in which signal attenuates by 5 dB and thereby to validate our measurement method, the time resolution of tens of ms is required (the time duration is reported to have the value of tens of ms in [11]). Because there is a tradeoff between the acquisition bandwidth and the time resolution (a wider acquisition bandwidth sacrifices the time resolution), we conduct the measurement in a smaller bandwidth than the IEEE 802.11ad WLAN channel bandwidth. In our measurement system, the measurement bandwidth of 10 MHz allowed us to obtain the temporal signal attenuation in a time resolution of around 20 ms.

The measurement was conducted under the condition that the AP transmits data frames to the STA as shown in Figure 1. The frame transmission was done by generating uplink traffic from the laptop connected to the AP with a gigabit Ethernet cable. The traffic was generated by Iperf3 [20].

For the sake of clarity of the discussion in the following sections, we show the signal representation. Let $r(t)$ be the representation of I-channel components of the 11ad WLAN signal converted by the down converter and let $b(t)$ be the impulse response of the acquisition band-pass filter in the spectrum analyzer. Then, the signal that is to be sampled by the A/D converter in the spectrum analyzer is represented by $y(t) = (r(t) + n(t)) * b(t)$, where $n(t)$ is the noise inherent in the measurement device and $*$ represents the convolution of two functions. Note that $r(t)$ is equivalent to 0 when the AP does not transmit any frames.

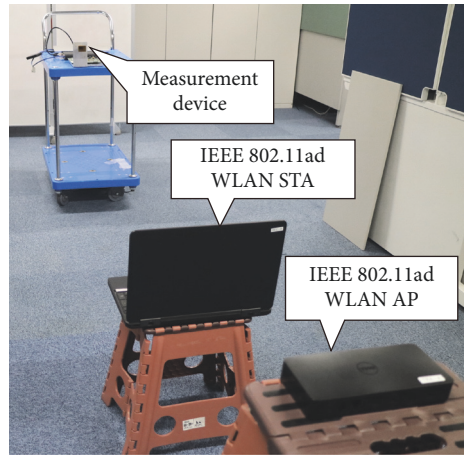

Figure 2: Measurement system.

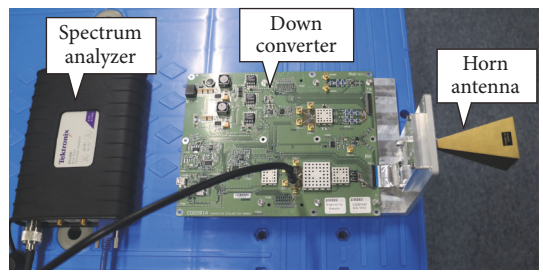

Figure 3: Measurement device.

3. Measurement Method of Temporal Signal Attenuation

3.1. Overview. Let the vector that identifies whether the AP transmits frames or not be denoted by $\mathbf{z}(t) = (z_0(t), z_1(t))^{\mathrm{T}}$, which is defined as

$$\mathbf{z}(t) := \begin{cases} (0,1)^{\mathrm{T}} & \text{if the AP transmits a frame,} \\ (1,0)^{\mathrm{T}} & \text{otherwise.} \end{cases} \tag{1}$$

Let $\mathscr{D}$ be the union of disjoint time intervals when the AP transmits frames, defined as

$$\mathscr{D} := \{t \mid z_1(t) = 1\}. \tag{2}$$

Let $\mathscr{D}(t_m) := \mathscr{D} \cap [t_m, t_m + KT]$ be the time duration when the AP transmitted frames in the sampling window $[t_m, t_m + KT]$, where t_m denotes the time at which the analyzer starts the mth sweep, while K and T denote the number of samples and the sampling period, respectively; therefore, $t_m + KT$ denotes the time at which the analyzer ends the sweep. The timing of sweeps is depicted in Figure 4. Note that the time length KT for which the analyzer sweeps (it is 200 μs in the measurements) is shorter than the interval $t_{m+1} - t_m$ between successive sweeps (it is 20 ms).

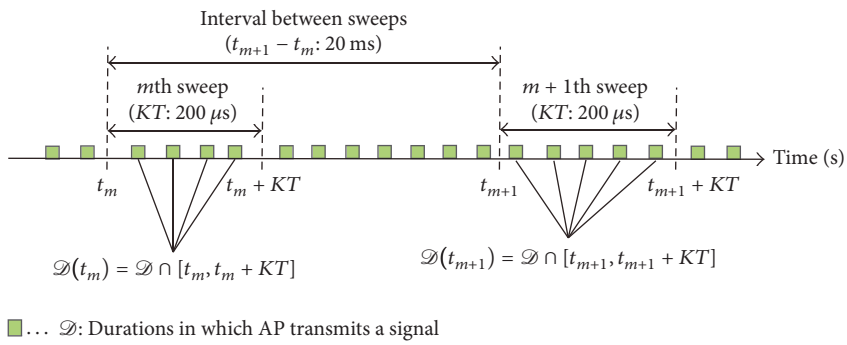

Figure 4: Timing of sweeps.

Our goal is to obtain the time-dependent attenuation value $A(t_m)$ given by

$$A(t_m) = \frac{P(t_m)}{P(t_1)}, \tag{3}$$

where $P(t_m)$ is the mean power of the measured signal, given by

$$P(t_m) = \frac{\int_{D(t_m)} |y(t)|^2 \, \mathrm{d}t}{\int_{D(t_m)} \mathrm{d}t}, \tag{4}$$

that is, the mean value of the power samples $p_m[k_m] := |y(t_m+k_mT)|^2$ for $k_m \in \{1, \ldots, K\}$ taken only if $z_1(t_m+k_mT) = 1$. $P(t_m)$ for $m > 1$ is obtained in the possible presence of human bodies, while $P(t_1)$ is obtained in the absence of human bodies and is the reference used to compute the attenuation $A(t_m)$.

We calculate $A(t_m)$ by three steps: the BIC-based model selection, the HMM-based frame transmission state estimation, and averaging. First, BIC-based model selection decides which of a two-state HMM and a one-state model is more appropriate to be applied to the obtained data $\mathbf{p}_m = (p_m[1], \ldots, p_m[K])^{\mathrm{T}}$. Only when the two-state HMM is selected is the HMM-based frame transmission state estimation conducted. Then, we estimate whether $z_1(t_m + k_mT) = 1$ or not for $k_m \in \{1, \ldots, K\}$, that is, whether the AP transmitted frames or not at each sampling point. Finally, we calculate the average of $p_m[k_m]$ for k_m which is estimated to be $z_1(t_m + k_mT) = 1$.

3.2. HMM-Based Frame Transmission State Estimation

3.2.1. HMM-Based Estimation Scheme. Let $\mathbf{z}_m[k_m] = (z_{m,0}[k_m], z_{m,1}[k_m])^{\mathrm{T}}$ denote $\mathbf{z}(t_m + k_mT)$. The main purpose of this subsection is to decide whether $z_{m,1}[k_m] = 1$ or not for $k_m \in \{1, \ldots, K\}$. The decision is based on modeling the power observations $p_m[k_m]$ using a two-state HMM. We now consider that the two-state HMM is selected in the BIC-based model selection in advance. The model selection is discussed in Section 3.3.

An HMM is a statistical model that forms a sequence of observations whose distribution depends on a latent variable that follows a Markov chain. We now consider $\mathbf{z}_m[k_m]$ as the latent variable on which the distribution of $p_m[k_m]$ depends. We refer to the phenomenon that $z_{m,1}[k_m] = 1$ as *frame transmission state*; the phenomenon that $z_{m,1}[k_m] = 0$ is considered as *pausing state*. We assume that the distribution conditioned on $\mathbf{z}_m[k_m]$ is an exponential distribution; thus, the probability density functions of $p_m[k_m]$ conditioned on $\mathbf{z}_m[k_m]$ are given as follows:

$$\begin{aligned} p(p_m[k_m] \mid z_{m,0}[k_m] = 1) &= \lambda_0 \exp(-\lambda_0 p_m[k_m]), \\ p(p_m[k_m] \mid z_{m,1}[k_m] = 1) &= \lambda_1 \exp(-\lambda_1 p_m[k_m]), \end{aligned} \tag{5}$$

where λ_i for $i \in \{0, 1\}$ denotes the parameter of the exponential distribution when $z_{m,i}[k_m] = 1$. The assumption is validated by the experimental results.

We estimate the most likely sequence of the latent variables utilizing Viterbi algorithm. Viterbi algorithm requires the parameters of the HMM which include λ_i, transition probabilities, and initial state probabilities. Because of the lack of the knowledge of the true parameters, we estimate the most likely parameters using expectation maximization (EM) algorithm. Each algorithm is described in detail as follows.

3.2.2. Parameter Estimation. We estimate the parameters of the HMM given by $\boldsymbol{\theta} = (\lambda_0, \lambda_1, q_{0,0}, q_{0,1}, q_{1,0}, q_{1,1}, \pi_0, \pi_1)^{\mathrm{T}}$, where $q_{i,j}$ for $i \in \{0, 1\}$ and $j \in \{0, 1\}$ represents the transition probability of a latent variable that is defined as $\mathbb{P}(z_{m,j}[k_m + 1] = 1 \mid z_{m,i}[k_m] = 1)$; π_i represents the initial state probability that is defined as $\mathbb{P}(z_{m,i}[1] = 1)$.

The estimation utilizes EM algorithm [21]. The EM algorithm derives the estimator $\widehat{\boldsymbol{\theta}}$ maximizing a likelihood $p(\mathbf{p}_m \mid \boldsymbol{\theta})$ via the iteration of E-step and M-step. The E-step derives the expectation of $\ln p(\mathbf{p}_m, \mathbf{Z}_m \mid \boldsymbol{\theta})$ under the posterior distribution of $\mathbf{Z}_m := (\mathbf{z}_m[1], \ldots, \mathbf{z}_m[K])$ and a current estimator:

$$\boldsymbol{\theta}^{(n)} = \left(\lambda_0^{(n)}, \lambda_1^{(n)}, q_{0,0}^{(n)}, q_{0,1}^{(n)}, q_{1,0}^{(n)}, q_{1,1}^{(n)}, \pi_0^{(n)}, \pi_1^{(n)}\right)^{\mathrm{T}}, \tag{6}$$

where n is an iteration number. The M-step derives the estimator:

$$\begin{aligned} \boldsymbol{\theta}^{(n+1)} = \Big(&\lambda_0^{(n+1)}, \lambda_1^{(n+1)}, q_{0,0}^{(n+1)}, q_{0,1}^{(n+1)}, q_{1,0}^{(n+1)}, q_{1,1}^{(n+1)}, \pi_0^{(n+1)}, \\ &\pi_1^{(n+1)}\Big)^{\mathrm{T}}, \end{aligned} \tag{7}$$

which maximizes the expectation. Details of each step are described later. The iteration is guaranteed to converge to the locally optimal estimator $\widehat{\boldsymbol{\theta}}$ [21].

The goal of the E-step is to derive the expectation of $\ln p(\mathbf{p}_m, \mathbf{Z}_m \mid \boldsymbol{\theta})$ under the posterior distribution of $\mathbf{Z}_m$ given $\mathbf{p}_m$ and the current estimator $\boldsymbol{\theta}^{(n)}$. Consider the expectation $Q(\boldsymbol{\theta}, \boldsymbol{\theta}^{(n)})$, which is described as follows:

$$\begin{aligned} Q\left(\boldsymbol{\theta}, \boldsymbol{\theta}^{(n)}\right) &:= \mathbb{E}_{\mathbf{Z}_m}\left[\ln p\left(\mathbf{p}_m, \mathbf{Z}_m \mid \boldsymbol{\theta}\right) \mid \mathbf{p}_m, \boldsymbol{\theta}^{(n)}\right] \\ &= \sum_{\mathbf{Z}_m} p\left(\mathbf{Z}_m \mid \mathbf{p}_m, \boldsymbol{\theta}^{(n)}\right) \ln p\left(\mathbf{p}_m, \mathbf{Z}_m \mid \boldsymbol{\theta}\right). \end{aligned} \tag{8}$$

As in [21], the expectation is given as follows:

$$\begin{aligned} &Q\left(\boldsymbol{\theta}, \boldsymbol{\theta}^{(n)}\right) \\ &\quad = \sum_{i=0}^{1} \gamma\left(z_{m,i}[1]\right) \ln \pi_i \\ &\qquad + \sum_{k_m=2}^{K} \sum_{j=0}^{1} \sum_{i=0}^{1} \xi\left(z_{m,j}[k_m-1], z_{m,i}[k_m]\right) \ln q_{j,i} \\ &\qquad + \sum_{k_m=1}^{K} \sum_{i=0}^{1} \gamma\left(z_{m,i}[k_m]\right) \\ &\qquad \cdot \ln p\left(p_m[k_m] \mid z_{m,i}[k_m] = 1, \boldsymbol{\theta}^{(n)}\right), \end{aligned} \tag{9}$$

where

$$\begin{aligned} &\gamma\left(z_{m,i}[k_m]\right) := \mathbb{E}_{\mathbf{z}_m[k_m]}\left[z_{m,i}[k_m] \mid \mathbf{p}_m, \boldsymbol{\theta}^{(n)}\right] \\ &\quad = \sum_{\mathbf{z}_m[k_m]} z_{m,i}[k_m]\, p\left(\mathbf{z}_m[k_m] \mid \mathbf{p}_m, \boldsymbol{\theta}^{(n)}\right), \\ &\xi\left(z_{m,j}[k_m-1], z_{m,i}[k_m]\right) \\ &\quad := \mathbb{E}_{\mathbf{z}_m[k], \mathbf{z}_m[k-1]}\left[z_{m,j}[k_m-1]\, z_{m,i}[k] \mid \mathbf{p}_m, \boldsymbol{\theta}^{(n)}\right] \\ &\quad = \sum_{\mathbf{z}_m[k_m-1]} \sum_{\mathbf{z}_m[k_m]} z_{m,j}[k_m-1]\, z_{m,i}[k_m] \\ &\qquad \cdot p\left(\mathbf{z}_m[k_m-1], \mathbf{z}_m[k_m] \mid \mathbf{p}_m, \boldsymbol{\theta}^{(n)}\right). \end{aligned} \tag{10}$$

These expectations, $\gamma(z_{m,i}[k_m])$ and $\xi(z_{m,j}[k_m-1], z_{m,i}[k_m])$, are derived via the forward-backward algorithm [21].

The M-step derives the revised estimator $\boldsymbol{\theta}^{(n+1)}$ that maximizes $Q(\boldsymbol{\theta}, \boldsymbol{\theta}^{(n)})$, which satisfies

$$\boldsymbol{\theta}^{(n+1)} = \arg\max_{\boldsymbol{\theta}} \quad Q\left(\boldsymbol{\theta}, \boldsymbol{\theta}^{(n)}\right). \tag{11}$$

The maximization with respect to π_i, $q_{i,j}$ $\forall i, j$ is achieved using appropriate Lagrange multipliers with the results [21]:

$$\begin{aligned} \pi_i^{(n+1)} &= \frac{\gamma\left(z_{m,i}[1]\right)}{\sum_{j=0}^{1} \gamma\left(z_{m,j}[1]\right)}, \\ q_{j,i}^{(n+1)} &= \frac{\sum_{k_m=2}^{K} \xi\left(z_{m,j}[k_m-1], z_{m,i}[k_m]\right)}{\sum_{i=0}^{1} \sum_{k_m=2}^{K} \xi\left(z_{m,j}[k_m-1], z_{m,i}[k_m]\right)}. \end{aligned} \tag{12}$$

The maximization with respect to λ_i, $\forall i$, is achieved via partial derivative with respect to λ_i, which results in

$$\lambda_i^{(n+1)} = \frac{\sum_{k_m=1}^{K} \gamma\left(z_{m,i}[k_m]\right)}{\sum_{k_m=1}^{K} p_m[k_m]\, \gamma\left(z_{m,i}[k_m]\right)}. \tag{13}$$

These steps are iterated until the convergence condition, $|Q(\boldsymbol{\theta}^{(n+1)}, \boldsymbol{\theta}^{(n)}) - Q(\boldsymbol{\theta}^{(n)}, \boldsymbol{\theta}^{(n-1)})| < \epsilon_0$, is satisfied, where ϵ_0 is the predefined tolerance. We set the tolerance to be 10^{-2}, which is much smaller than the likelihoods that have a value of the order of 10^5 in these experiments.

3.2.3. Estimation of a Sequence of Latent Variables. The goal to estimate the most likely sequence of latent variables is achieved via Viterbi algorithm. Viterbi algorithm seeks for the sequence of latent variables $\widehat{\mathbf{Z}}_m$, which is described as

$$\widehat{\mathbf{Z}}_m = \arg\max_{\mathbf{Z}_m} \quad p\left(\mathbf{p}_m, \mathbf{Z}_m \mid \widehat{\boldsymbol{\theta}}\right). \tag{14}$$

Viterbi algorithm in the HMM works as maximum likelihood detection of convolutional codes [22]. Consider the trellis diagram, where, for all values k_m, all possible latent variables in the k_mth sampling point are deployed as the nodes at the trellis depth k_m and all the nodes at the trellis depth k_m are connected to all the nodes at the trellis depth $k_m + 1$. $\widehat{\mathbf{Z}}_m = (\widehat{\mathbf{z}}_m[1], \ldots, \widehat{\mathbf{z}}_m[K])$ is achieved by seeking for the trellis path maximizing path metric, defining the branch metric from the $(i+1)$th node at the depth k_m to the $(j+1)$th node at the depth $k_m + 1$, $B_{k_m}^{(i\to j)}$, as follows:

$$\begin{aligned} B_{k_m}^{(i\to j)} &= \ln\left\{p\left(\mathbf{z}_{m,j}[k_m+1] = 1 \mid \mathbf{z}_{m,i}[k_m] = 1, \widehat{\boldsymbol{\theta}}\right)\right. \\ &\quad \left. \cdot\, p\left(p_m[k_m+1] \mid \mathbf{z}_{m,j}[k_m+1] = 1, \widehat{\boldsymbol{\theta}}\right)\right\}. \end{aligned} \tag{15}$$

3.2.4. Model Verification. We show that Viterbi algorithm can estimate latent variables in each sampling point. Using the results, we validate the assumption that $p_m[k_m]$ in each state follows the exponential distribution.

Figure 5 shows an example of the estimation of latent variables. This shows that each latent variable is consecutive for a certain duration. This result agrees with the fact that the AP transmits a frame in a certain duration: from the start of transmission to the end.

Figure 6 shows the cumulative frequencies of $p_m[k_m]$ in each estimated state and theoretical cumulative distribution function (CDF) of each exponential distribution. The parameters of each exponential distribution are estimated via EM algorithm. This figure shows that the distribution of $p_m[k_m]$ in each state coincides with the theoretical CDF, which also shows the validity of the assumption that $p_m[k_m]$ in each state follows the exponential distribution.

3.3. BIC-Based Model Selection. In the previous subsection, we considered that fitting the data using a two-state model is more appropriate than using a one-state model. However, there exist data in which no frames are observed because the AP did not transmit any frames for the time duration

input: power observations $\mathbf{P} = (\mathbf{p}_1, \ldots, \mathbf{p}_M)$
output: time series of signal attenuation $(A(t_1), \ldots, A(t_M))^{\mathrm{T}}$
(1) **for** $m \in \{1, \ldots, M\}$ **do**
(2) conduct maximum likelihood estimation of a one-state exponential distribution model and calculate BIC, BIC_1
(3) conduct EM algorithm in a two-state HMM and compute BIC, BIC_2
(4) **if** $\mathrm{BIC}_2 < \mathrm{BIC}_1$ **then**
(5) estimation of the maximum-likely latent variables $\widehat{\mathbf{Z}}_m$ using Viterbi algorithm
(6) $P_m \leftarrow$ average of $p_m[k_m]$ for $\forall k_m \in \{k \in \{1, \ldots, K\} \mid \widehat{z}_{m,1}[k] = 1\}$
(7) $A(t_m) \leftarrow P_m / P_1$
(8) **end if**
(9) **end for**

Algorithm 1: Procedure for measuring temporal signal attenuation in mmWave WLAN.

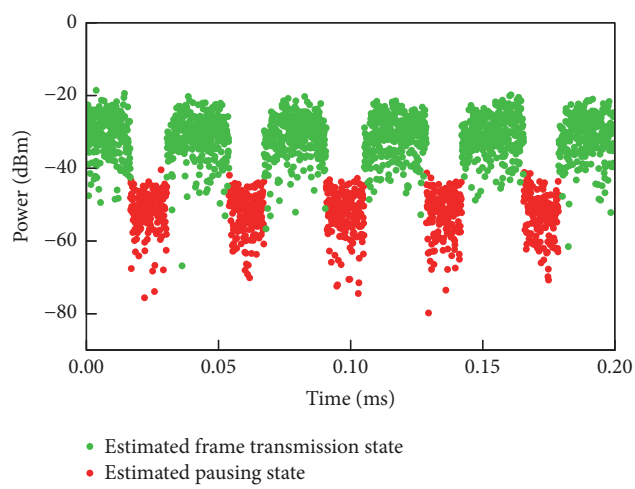

Figure 5: Example of the estimate of whether the AP transmitted frames or not.

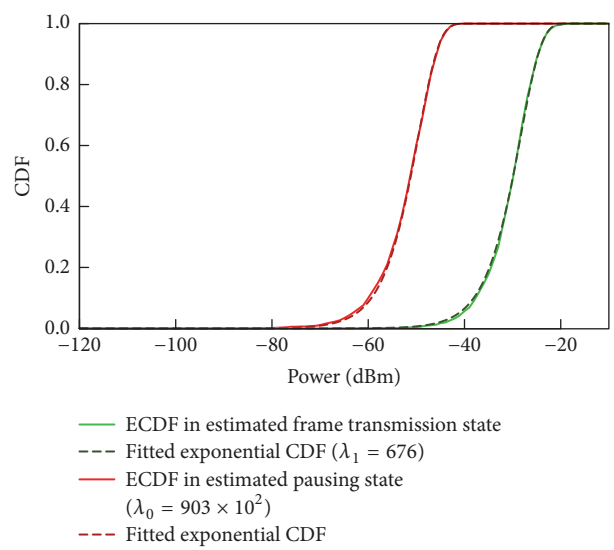

Figure 6: Cumulative frequencies of power observations in each state and CDF of fitted exponential distributions.

of $[t_m, t_m + KT]$ (as an alternative approach, we can set the sampling rate and the number of samples per sweep so that at least one beacon signal is received. Note that the beacon interval of the AP we employed is 1.1 ms [11]). In this case, applying a one-state model, where $p_m[k_m]$ follows an identical exponential distribution, is more appropriate because applying a two-state model causes model overfitting and consequent invalid calculation of $A(t_m)$. If a two-state HMM is applied in this case, there exists $k_m \in \{1, \ldots, K\}$ for which $\widehat{z}_{m,1}[k] = 1$ although the truth is that $\widehat{z}_{m,1}[k_m] = 0\ \forall k_m \in \{1, \ldots, K\}$. Thus, it is required that which model to be appropriate is decided and that if the one-state model is estimated to be appropriate, we decide that we do not calculate $A(t_m)$.

To decide which model to be appropriate, we utilize BIC [21]. BIC is given as follows:

$$\mathrm{BIC} = -L\left(\widehat{\boldsymbol{\theta}}\right) + \frac{d}{2} \ln K, \tag{16}$$

where $L(\cdot)$ denotes the log-likelihood function and d is the number of parameters that are required to describe each model. In the two-state HMM, $d = 5$; that is, the parameters are λ_0, λ_1, $q_{0,0}$, $q_{1,0}$, and π_0. Note that $q_{0,1}$, $q_{1,1}$, and π_1 are not counted because these parameters are decided deterministically from $q_{0,0}$, $q_{1,0}$, and π_0, respectively. In the one-state model, $d = 1$. $\widehat{\boldsymbol{\theta}}$ is the vector containing the model parameters with maximum likelihood. The model whose BIC is smaller than that of the counterpart is applied.

The second term of BIC is interpreted to be the penalty of increasing the number of model parameters. The penalty of BIC is more than that of Akaike information criterion (AIC) [23], which is a reason why we adopt BIC. BIC tends not to select the two-state model that has more parameters and therefore prevents from model overfitting.

3.4. Procedure of Calculating Time-Varying Signal Attenuation. We summarized the procedure of the calculation of $A(t_m)$ in Algorithm 1. First, we compute BIC of each model. BIC of the one-state exponential distribution model, BIC_1, is calculated via maximum likelihood estimation; that of the two-state HMM, BIC_2, is calculated via EM algorithm. If $\mathrm{BIC}_2 < \mathrm{BIC}_1$, Viterbi algorithm is conducted to estimate the latent variables and then $A(t_m)$ is calculated by averaging $p_m[k]$ in frame

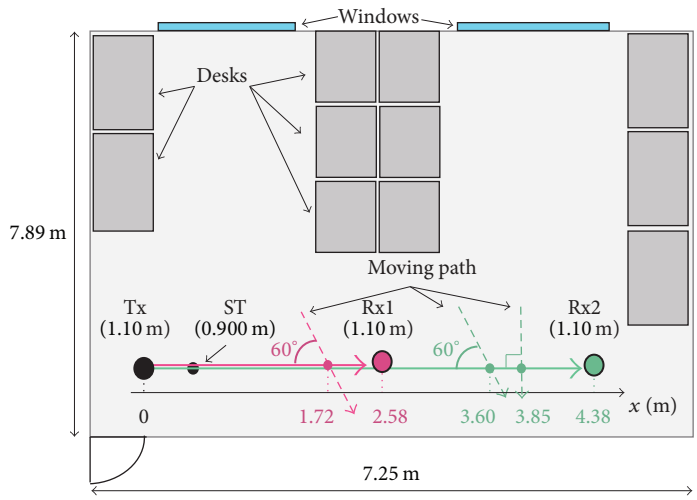

Figure 7: Top view of measurement environment with the moving path and positions of the AP, STA, and measurement device, denoted by TX, ST, and RX1 or RX2, respectively. Values in parentheses indicate the height of each device.

transmission state. If not, it is decided that the calculation of $A(t_m)$ is not conducted because the AP did not transmit any frames.

4. Measurement of Time-Varying Attenuation in IEEE 802.11ad WLAN

4.1. Objective. The main objective of the measurements is to validate the measurement method by demonstrating the consistency in quantities associated with the signal attenuation under a similar condition to that in the previous report [11]; additional measurements in other conditions are out of the scope of this paper. As in [11], we measured the duration $t_{\text{decay,5 dB}}$ in which signal attenuation level increases from 0 dB to 5 dB, the duration $t_{\text{rise,5 dB}}$ in which signal attenuation level decreases from 5 dB to 0 dB, and the mean signal attenuation A_{mean} in the interval $[t_{\text{b}} + (t_{\text{e}} - t_{\text{b}})/3, t_{\text{e}} - (t_{\text{e}} - t_{\text{b}})/3]$, where t_{b} and t_{e} represent, respectively, the last zero crossing time before a shadowing event and the first zero crossing time after the shadowing event.

4.2. Experiment Description. The measurements were conducted in a similar experimental scenario to the previous report [11] in order to compare our results with the results in the report. The moving paths of the pedestrian were kept fixed as in Figure 7, which are similar moving paths to those in the report.

Figure 7 also depicts the deployment of the measurement equipment. The AP and STA were kept fixed at the positions TX and ST, whereas the measurement device was placed at the positions RX1 and RX2. The separation distances between TX and RX1 and between TX and RX2 were 2.58 m and 4.38 m, respectively. The height of the AP and the measurement device was 1.10 m; that of the STA was 0.90 m.

4.3. Experimental Results. Figure 8 shows an example of the time series of measured signal attenuation induced by human blockage. The signal attenuation level oscillates by up to 2 dB

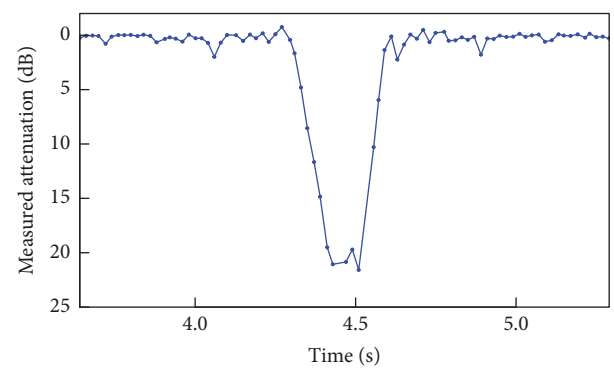

Figure 8: Time series of measured attenuation of signal transmitted by IEEE 802.11ad AP induced by human blockage.

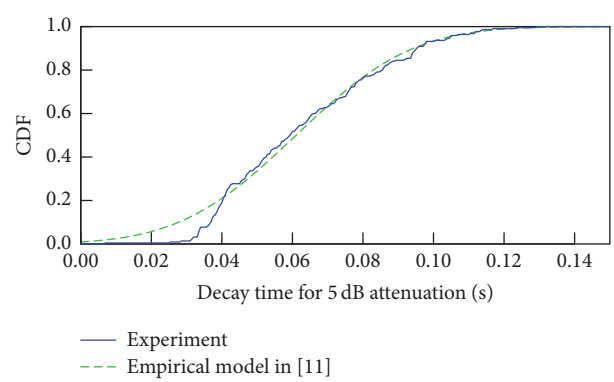

Figure 9: CDF of decay time for 5 dB attenuation, $t_{\text{decay,5 dB}}$.

before and after the signal attenuates. This is in agreement with a knife edge diffraction theory [24].

Figure 9 shows the CDF of the decay time $t_{\text{decay,5 dB}}$. The empirical model in [11] is the Gaussian distribution with the mean of 0.061 s and the standard deviation of 0.026 s.

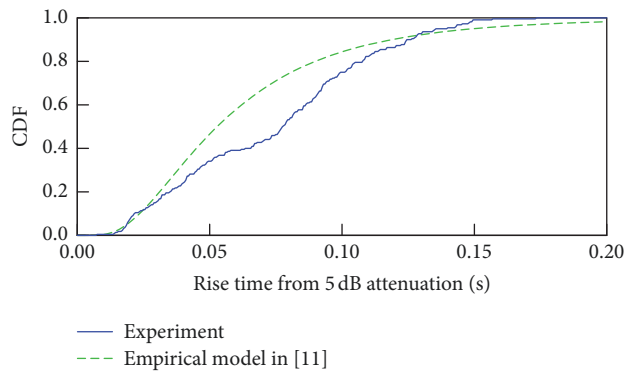

Figure 10: CDF of rise time from 5 dB attenuation, $t_{\text{rise},5\,\text{dB}}$.

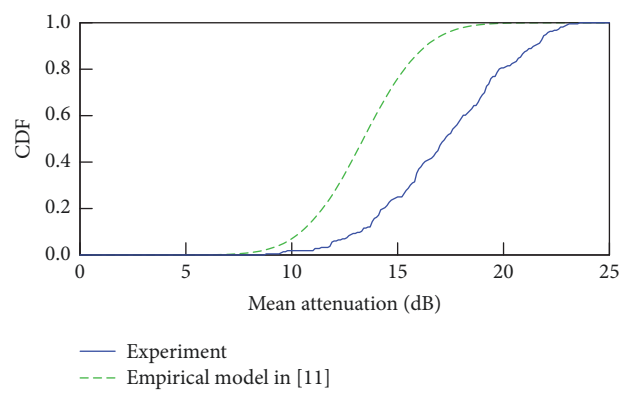

Figure 11: CDF of mean signal attenuation while pedestrian is blocking the LOS path, A_{mean}.

The measured cumulative frequency of $t_{\text{decay},5\,\text{dB}}$ coincides with the model. In fact, the model cannot be rejected by the Kolmogorov-Smirnov test [25] with a significance level of 1%. Thus, in terms of the decay time $t_{\text{decay},5\,\text{dB}}$, the empirical model is valid for the IEEE 802.11ad WLAN signals transmitted by a commercially available AP with a consumer-grade array antenna as well as ones transmitted by a transmitter with a horn antenna.

Figure 10 shows the CDF of the rise time t_{rise}. The empirical model in [11] is the log-normal distribution with the log mean of −2.94 and the log standard deviation of 0.63. We can see that although there is a difference in the shape of the CDF, our results are consistent with the empirical model in that the rise time ranges from 0.02 s to 0.15 s.

Figure 11 shows the CDF of the mean signal attenuation A_{mean}. The empirical model in [11] is the Gaussian distribution with the mean of 13 dB and the standard deviation of 2.0 dB. This result shows that the signal in IEEE 802.11ad WLAN attenuates about 4.0 dB more than the signal in [11]. These differences might be attributable to the difference between the transmit antennas: the horn antenna employed in the report and the array antenna packed in the AP and the position at which the pedestrian crossed the LOS path (the report in [15] demonstrated that blockage at nearer positions to the receiver causes the higher signal attenuation in directional communications).

5. Conclusion

This paper discussed a measurement method of time-varying attenuation of signals transmitted by a commercially available IEEE 802.11ad WLAN AP caused by human blockage. We applied a two-state HMM in order to estimate whether the AP transmitted signals or not in each sampling point. We also presented the BIC-based model selection that decides which of one-state model and two-state model is to be applied. The two-state HMM-based estimation showed the valid results: both the sampling points estimated to be in frame transmission state and those estimated to be in pausing state are consecutive for a certain duration, which is consistent with a transmission mechanism of IEEE 802.11ad WLAN APs. The measurements are validated in that the measured time-varying signal attenuation is in an agreement with knife edge diffraction theory. The measurements are also validated in that the statistical characteristics of the duration in which the signal transmitted by the AP attenuates by 5 dB were consistent with the existing statistical model. On the other hand, the measurement results are different from the existing report in terms of the mean attenuation while a human is blocking a LOS path.

Disclosure

This paper was presented in part at IEEE 86th Vehicular Technology Conference (VTC2017-Fall) [26].

Conflicts of Interest

The authors declare that they have no conflicts of interest.

Acknowledgments

The authors would like to thank Dr. Katsuyuki Haneda at Aalto University for his advice. This work was supported in part by JSPS KAKENHI (Grant no. JP17H03266) and by KDDI Foundation.

References

[1] E. Perahia and M. X. Gong, "Gigabit wireless LANs," *ACM SIGMOBILE Mobile Computing and Communications Review*, vol. 15, no. 3, p. 23, 2011.

[2] X. Tie, K. Ramachandran, and R. Mahindra, "On 60 GHz wireless link performance in indoor environments," *Lecture Notes in Computer Science (including subseries Lecture Notes in Artificial Intelligence and Lecture Notes in Bioinformatics): Preface*, vol. 7192, pp. 147–157, 2012.

[3] K. Haneda, "Channel models and beamforming at millimeter-wave frequency bands," *IEICE Transactions on Communications*, vol. E98B, no. 5, pp. 755–772, 2015.

[4] K. Sakaguchi, E. M. Mohamed, H. Kusano et al., "Millimeter-wave wireless LAN and its extension toward 5G heterogeneous networks," *IEICE Transactions on Communications*, vol. E98B, no. 10, pp. 1932–1948, 2015.

[5] T. Nitsche, G. Bielsa, I. Tejado, A. Loch, and J. Widmer, "Boon and bane of 60 GHz networks: Practical insights into beamforming, interference, and frame level operation," in *Proceedings*

of the 11th ACM Conference on Emerging Networking Experiments and Technologies, CoNEXT 2015, Germany, December 2015.

[6] S. Collonge, G. Zaharia, and G. El Zein, "Influence of the human activity on wide-band characteristics of the 60 GHz indoor radio channel," *IEEE Transactions on Wireless Communications*, vol. 3, no. 6, pp. 2396–2406, 2004.

[7] Y. Oguma, T. Nishio, K. Yamamoto, and M. Morikura, "Implementation and evaluation of reactive base station selection for human blockage in mmWave communications," in *Proceedings of the 21st Asia-Pacific Conference on Communications, APCC 2015*, pp. 199–203, Kyoto, Japan, October 2015.

[8] M. Umehira, G. Saito, S. Wada, S. Takeda, T. Miyajima, and K. Kagoshima, "Feasibility of RSSI based access network detection for multi-band WLAN using 2.4/5GHz and 60GHz," in *Proceedings of the 2014 International Symposium on Wireless Personal Multimedia Communications, WPMC 2014*, pp. 243–248, Sydney, Australia, September 2014.

[9] Y. M. Tsang and A. S. Y. Poon, "Detecting human blockage and device movement in mmwave communication system," in *Proceedings of the 54th Annual IEEE Global Telecommunications Conference: "Energizing Global Communications", GLOBECOM 2011*, Houston, USA, December 2011.

[10] "Wireless LAN medium access control (MAC) and physical layer (PHY) specification, IEEE Std. 802.11ad-2012".

[11] M. Jacob, C. Mbianke, and T. Kürner, "A dynamic 60 GHz radio channel model for system level simulations with MAC protocols for IEEE 802.11ad," in *Proceedings of the 14th IEEE International Symposium on Consumer Electronics, ISCE 2010*, Braunschweig, Germany, June 2010.

[12] M. Jacob, S. Priebe, A. Maltsev, A. Lomayev, V. Erceg, and T. Kurner, "A ray tracing based stochastic human blockage model for the IEEE 802.11ad 60 GHz channel model," in *Proceedings of the the 5th European Conference on Antennas and Propagation (EUCAP '11)*, pp. 3084–3088, IEEE, Rome, Italy, April 2011.

[13] T. Wang, M. Umehira, H. Otsu, S. Takeda, T. Miyajima, and K. Kagoshima, "A twin cylinder model for moving human body shadowing in 60GHz WLAN," in *Proceedings of the 21st Asia-Pacific Conference on Communications, APCC 2015*, pp. 188–192, Japan, October 2015.

[14] M. Jacob, S. Priebe, M. Peter, and M. Wisozki, "Fundamental analyses of 60 GHz human blockage," in *Proceedings of the IEEE EuCAP 2013*, pp. 117–121, IEEE, Gothenburg, Sweden, 2013.

[15] G. R. Maccartney, S. Deng, S. Sun, and T. S. Rappaport, "Millimeter-wave human blockage at 73 GHz with a simple double knife-edge diffraction model and extension for directional antennas," in *Proceedings of the 84th IEEE Vehicular Technology Conference, VTC Fall 2016*, Canada, September 2016.

[16] G. R. MacCartney and T. S. Rappaport, "A flexible millimeter-wave channel sounder with absolute timing," *IEEE Journal on Selected Areas in Communications*, vol. 35, no. 6, pp. 1402–1418, 2017.

[17] P. Karadimas, B. Allen, and P. Smith, "Human body shadowing characterization for 60-GHz indoor short-range wireless links," *IEEE Antennas and Wireless Propagation Letters*, vol. 12, pp. 1650–1653, 2013.

[18] A. J. Coulson, "Spectrum sensing using hidden Markov modeling," in *Proceedings of the 2009 IEEE International Conference on Communications, ICC 2009*, pp. 1–6, Dresden, Germany, June 2009.

[19] K. Haghighi, E. G. Ström, and E. Agrell, "On optimum causal cognitive spectrum reutilization strategy," *IEEE Journal on Selected Areas in Communications*, vol. 30, no. 10, pp. 1911–1921, 2012.

[20] "Iperf," https://iperf.fr/.

[21] C. Bishop, *Pattern Recognition and Machine Learning*, Springer, Berlin, Germany, 2010.

[22] A. Goldsmith, *Wireless communications*, Cambridge University Press, 2004.

[23] H. Akaike, "A New Look at the Statistical Model Identification," *IEEE Transactions on Automatic Control*, vol. 19, no. 6, pp. 716–723, 1974.

[24] S. R. Saunders and A. A. Zavala, "Antennas and propagation for wireless communication systems," Wiley, 2007.

[25] A. Papoulis and S. Pillai, *Probability, Random Variables and Stochastic Processes*, McGraw-Hill, New York, NY, USA, 4th edition, 2002.

[26] Y. Koda, K. Yamamoto, T. Nishio, and M. Morikura, "Time Series Measurement of IEEE 802.11ad Signal Power Involving Human Blockage with HMM-Based State Estimation," in *Proceedings of the 2017 IEEE 86th Vehicular Technology Conference (VTC-Fall)*, pp. 1–5, IEEE, Toronto, Canada, September 2017.